Calcium fluoride on Si(001): Adsorption mechanisms and epitaxial growth modes

L. Pasquali,[1] S. M. Suturin,[2] V. P. Ulin,[2] N. S. Sokolov,[2] G. Selvaggi,[1] A. Giglia,[1,3] N. Mahne,[3] M. Pedio,[3] and S. Nannarone[1,3]

[1]*Dipartimento di Ingegneria dei Materiali e dell'Ambiente, Università di Modena e Reggio Emilia, Via Vignolese 905, 41100-Modena, Italy*

[2]*Ioffe Physical-Technical Institute, RAS, Solid State Optics Department, 26 Polytechnicheskaya str., 194021 St. Petersburg, Russia*

[3]*INFM-CNR-TASC Laboratory, s.s. 14, km 163.5 in AREA Science Park, 34012 Basovizza (TS), Italy*

(Received 31 March 2005; revised manuscript received 1 June 2005; published 28 July 2005)

Growth of CaF_2 on Si(001) is studied as a function of the substrate temperature during deposition for coverages from fraction of a monolayer (ML) up to several monolayers. Structural and morphological studies using atomic force microscopy, low-energy electron diffraction, and reflection high-energy electron diffraction are combined with measurements of core-level photoemission and x-ray absorption. Bonding between CaF_2 molecules and Si(001) substrates is followed by monitoring core-level shifts and x-ray absorption line shape. It is found that a dissociative reaction occurs at high deposition temperatures (~750 °C), giving rise to a 1-ML-thick uniform wetting layer, which is bonded with the substrate through Ca atoms. This wetting layer changes the surface periodicity from double domain $2\times1+1\times2$ to single domain 3×1. Three-dimensional CaF_2 elongated islands develop on top of the wetting layer, with their (110) planes parallel to the Si surface plane. At temperatures below 600 °C no dissociative reaction takes place for CaF_2; nanodimensional islands develop in the form of rectangular-based huts. The crystallographic orientation of these islands is parallel to that of the Si(001) substrate. The data are compared to results obtained on CaF_2 deposited on Si(111).

DOI: 10.1103/PhysRevB.72.045448 PACS number(s): 61.14.Hg, 79.60.Jv, 79.60.Bm

I. INTRODUCTION

Nowadays, the reliability and precision achieved by epitaxial deposition techniques together with a long-term and mature knowledge in the field of surface and interface science have made it possible to grow by design artificial low-dimensional structures (nanodots and nanowires) onto semiconductors, exploiting the natural tendency of materials to aggregate in different modes according to the preparation conditions. The atomic geometrical arrangement in these nanostructures, their morphology, and properties strongly depend on the growth parameters which are chosen: substrate surface orientation and smoothness, growth temperature, and deposition rate. The growth mode can thus be routed through "self-assembling" of structures which form spontaneously and evolve under kinetic or thermodynamic control with a fine adjust of the different growth variables.[1–3]

Here we report on the growth of calcium fluoride nanostructures on Si(001) as a function of substrate temperature and evaporation rate during deposition in ultrahigh vacuum. Calcium fluoride has always been considered as an interesting and prototypical insulating material to be grown epitaxially on silicon single-crystal surfaces.[4] Due to the small lattice mismatch between the two materials (0.6% at room temperature), CaF_2 films of good crystal quality can be grown by molecular beam epitaxy (MBE) on silicon. CaF_2 has very good insulating properties and optical transmission in the range of infrared and visible radiation. Epitaxial films of CaF_2 on Si(111), grown at elevated temperatures in UHV conditions, have often been recognized as promising candidates for substituting SiO_2 in metal-oxide-semiconductor (MOS) technology and in the fabrication of epitaxial multilayer structures,[5,6] with possible applications in microelectronics and optoelectronics. Furthermore, CaF_2 films on Si, if properly doped with rare-earth ions, can provide solid-state light emitters in the infrared and visible light ranges.[7,8] This system can also be considered as a prototype for the study of the atomic and electronic structure of the interface between a polar insulator with ionic bonding and an elemental semiconductor with covalent bonding. In fact, the character of the bonding changes from covalent Si—Si to ionic Ca-F within the interface region and induces strong modifications in the electronic band structure, which depends on the stoichiometry and nature of the bonds between different elements.

Stimulated by the number of potential applications, extensive studies of the growth of CaF_2 on silicon have been mainly carried out on Si(111).[4,9–12] Only a few attempts have been undertaken up to now to investigate the initial stages of CaF_2 growth on the technologically important Si(001) surface,[1,13,14] where anisotropic CaF_2 growth accompanied by the formation of quasi-one-dimensional islands was observed using transmission electron microscopy (TEM) and scanning tunneling microscopy (STM). These islands with nanometer-scale width can be attractive as insulating lines or for nanolithographic purposes. Moreover, learning to control the growth mode of fluorite onto Si(001) can lead to important technological applications—for example, in devices where CaF_2 is used as an inert insulating buffer layer for subsequent growth of different materials in a stacking sequence (e.g., ferromagnetic-antiferromagnetic multilayers).

In previous works[1,15–17] reflection high-energy electron diffraction (RHEED), atomic force microscopy (AFM), metastable deexcitation spectroscopy (MDS), and He I photoemission were used to investigate the growth mode of CaF_2 on Si(001). It has been pointed out that depending on the substrate temperature, deposition results in fluoride islands of different size and morphology. It was found that at

deposition temperatures below 600 °C, CaF_2 molecules tend to form uniformly distributed rectangular islands with a characteristic size below 10–20 nm and a height of 3–8 nm. The fluoride islands edges appear aligned with [110] or $[1\bar{1}0]$ directions of the substrate and grow with the [001] axis of CaF_2 aligned with the [001] axis of the substrate.

At deposition temperatures above 600–650 °C, CaF_2 molecules adsorbed at the surface dissociate, reacting and bonding to Si substrate atoms. This generates a wetting layer covering uniformly the surface. The dissociative reaction appears to terminate at one monolayer (1 ML) coverage. After this stage, on top of the wetting layer, elongated islands (stripes) develop, running along either the [110] or $[1\bar{1}0]$ substrate direction. It was found that the fluoride islands grow this time with their [110] axis aligned parallel to the [001] axis of the substrate.[13]

In the present work we intend to extend the previous analysis focusing on the mechanisms and chemical reactions that occur at the interface between the semiconductor and insulator with particular attention paid to the formation of the wetting layer at high temperature and to the role of the different growth parameters in the determination of growth modes. To this end, both structural and electronic properties probes have been applied. These include AFM, RHEED, low-energy electron diffraction (LEED), high-resolution photoemission at different photon energies, and x-ray absorption spectroscopy (XAS) using synchrotron radiation.

The paper is organized as follows: in Sec. II a brief description is given of the experimental procedures which were followed, in Sec. III the results related to the structure and morphology of the system are presented, the electronic properties are given in Sec. IV, a discussion and comments are reported in Sec. V, and Sec. VI is dedicated to the conclusions.

II. EXPERIMENT

The experiments were conducted in part at the Ioffe Physical-Technical Institute (St. Petersburg, Russia) and in part at the VUV-photoemission (BL 3.2R) (Ref. 18) and BEAR (BL 8.1L) (Ref. 19) beamlines at ELETTRA synchrotron radiation facility (Trieste, Italy).

In order to investigate growth modes and CaF_2/Si(001) epitaxial relations at different growth conditions (variable substrate temperatures and growth rates) RHEED and AFM were used. *In situ* RHEED measurements were carried out to monitor surface structures and growth modes; *ex situ* AFM was used to measure the surface morphology. The same growth conditions were employed both at the Ioffe and during synchrotron measurements, where the electronic properties of the system were studied.

CaF_2/Si(001) samples were grown by MBE in UHV conditions at a pressure below 1×10^{-7} Pa. Deposition of calcium fluoride was made using a homebuilt effusion cell, consisting of a graphite crucible loaded with small pieces of CaF_2 crystals. The crucible was heated by a tungsten grid filament up to about 1100 °C to produce a CaF_2 molecular beam. Due to strong ionic bonding, CaF_2 is known to sublime in the form of molecules, thus providing the stoichiometry of the beam.[20] The flux was calibrated by observing RHEED specular beam oscillations during first stages of CaF_2 growth on a Si(111) substrate (at the Ioffe) or with a quartz microbalance (at BEAR, VUV). The typical flux values used were in the range of 1–7 ML per minute [one nominal monolayer corresponding to 2.7 Å of thickness on Si(001)].

Silicon substrate heating was provided either by indirect heating, passing electric current through a heater filament located closely behind the substrate (at Ioffe, BEAR), or by direct heating, passing current through the substrate itself (at VUV). The substrate temperature was monitored with an optical or IR pyrometer and additionally with a tungsten-rhenium thermocouple (Ioffe).

Si(001) *n*-type substrates were used with a miscut angle of 1–3 mrad with respect to the (001) plane. They were cleaned prior to CaF_2 deposition, the procedure consisting of a standard chemical Shiraki treatment[21] followed by flashing the surface up to 1100–1200 °C in UHV conditions to remove silicon oxide.

The epitaxial relations and surface periodicity were measured at Ioffe during sample growth with a RHEED apparatus (15 keV electron gun) mounted on the MBE chamber. LEED was used to monitor the surface periodicity during synchrotron experiments. Since RHEED and LEED data were in most cases complementary in what concerns surface periodicity, here we will present only LEED data when the surface periodicity is of interest. RHEED data, instead, will be used to show lattice periodicity in the plane perpendicular to the surface. The latter can be obtained only when three-dimensional (3D) islands develop at the surface. These can be passed through by the *e* beam at grazing incidence, leading to typical 3D diffraction patterns (transmission spots).

The surface morphology of the CaF_2/Si(001) structures was measured in tapping (semicontact) mode with an ambient air P4-SPM NT-MDT atomic force microscope equipped with NSCS-11 cantilevers having a resonance frequency of 200–300 kHz. Typical resolution of the AFM was 10–20 nm laterally and 1–2 Å in the direction of the surface normal, depending on the sharpness of the cantilever tip.

Photoemission and x-ray absorption spectra were collected in different synchrotron experiments. High-resolution photoemission data were recorded with an Omicron EA125 electron analyzer at the 3.2 R VUV photoemission beamline both at normal and at 45° emission angles (with an angular acceptance of 8°). X-ray absorption spectra were taken at the 8.1 L BEAR beamline in total yield mode by measuring the drain current from the sample holder in *s*-type light polarization conditions (electric field vector perpendicular to the scattering plane) and with the light impinging at 70° with respect to the sample normal. Photoemission data were also taken at BEAR beamline with a double-pass Perkin-Elmer cylindrical mirror electron analyzer operated at constant pass energy. Energy resolutions varied according to the different spectral ranges investigated and beamline used.

All spectra were measured at room temperature, letting the samples cool down for a few minutes after the deposition step. Unless otherwise indicated, the evaporation rate employed for the samples used in the spectroscopic investigation was 2 ML per minute.

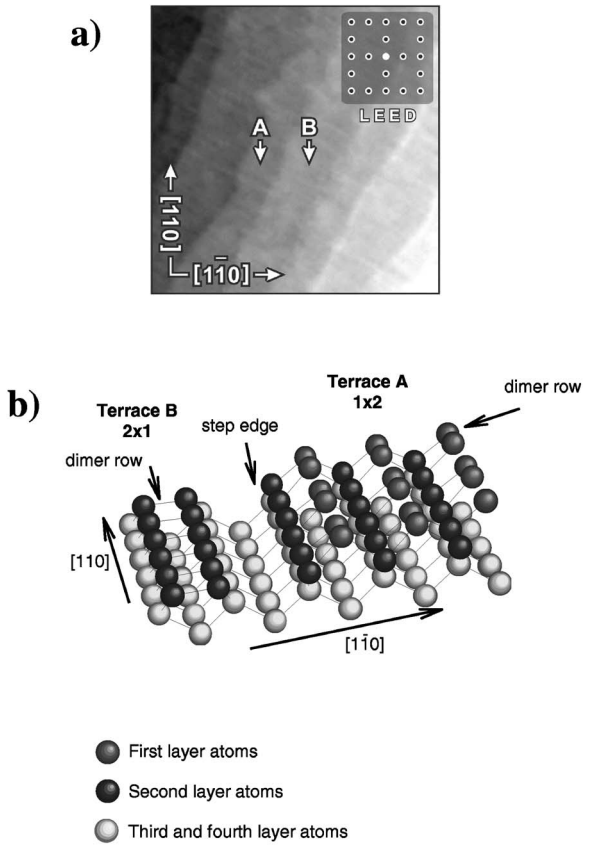

FIG. 1. (Color online) (a) Clean Si(001) substrate. AFM image shows flat terraces (*A* and *B*), separated by monoatomic steps. LEED pattern indicates a double-domain $2\times1+1\times2$ surface reconstruction. AFM scan dimensions 800 nm$\times$800 nm$\times$1.5 nm. (b) Perspective view of the Si(001) double-domain surface with monoatomic steps.

III. SURFACE MORPHOLOGY AND LATTICE STRUCTURE

A. Clean Si(001) surface

Figure 1 shows an AFM image of the Si(001) surface taken prior to calcium fluoride deposition. Clearly recognized on the surface are (001) terraces [labeled *A* and *B* in Fig. 1(a)] having a width of 50–150 nm and separated by single atomic steps of ~1.4 Å in height. The average terrace width is determined by the miscut angle of the Si substrates [1–3 mrad with respect to the (001) crystal plane].

On Si(001), each terrace is reconstructed in the form of dimer rows running along ⟨110⟩ directions and giving rise to a 2×1 periodicity.[22] For convenience, here we will denote the terrace as 2×1 when the dimer rows on it are running along the [110] direction [Fig. 1(b)]. On the terraces located one atomic step above and below, the dimer rows run in the perpendicular [1$\bar{1}$0] direction and the reconstruction is denoted as 1×2. Thus, the Si(001) surface is composed of two domains, consisting of 2×1 and 1×2 terraces. These have been labeled *B* and *A*, respectively, in Fig. 1(b). In the present case, the areas of 2×1 and 1×2 terraces with the dimer rows running orthogonal to each other on adjacent terraces are comparable, as estimated from the AFM images [see Fig. 1(a)]. This conclusion is supported by LEED observations showing half-order diffraction spots of comparable intensity in both orthogonal [110] and [1$\bar{1}$0] directions, which can be interpreted as a superposition of 2×1 and 1×2 reconstructions.

It should also be noted that unless the steps at the surface are oriented along ⟨100⟩-type directions, the two perpendicular ⟨110⟩-type directions at the surface are not equivalent with respect to the step edges. As a naming convention we define the [110] direction as the one that makes less than 45° with the step edges [as presented in Fig. 1(b)].

B. High-temperature growth

After deposition of ~0.1 ML of CaF_2 with the substrate held at 770 °C, narrow nanostripes appear running along [110] and [1$\bar{1}$0] directions [Fig. 2(a)]. Each nanostripe is confined within a single terrace, not propagating beyond the step edges. The step edges themselves appear to be modified with respect to the clean Si surface—at the point where a nanostripe arrives to the up-the-steps edge of the terrace, the step edge retreats, as if the propagating nanostripe consumed silicon atoms from the upper terrace. In opposite, no nanostripes are observed to modify the down-the-steps terrace edge.

LEED patterns obtained for less than 1 ML of coverage [see the inset in Fig. 2(a)] can be interpreted as showing a mixture of 2×1, 1×2, 3×1, and 1×3 superstructures. The 2×1 and 1×2 patterns apparently belong to areas of Si(001) surface still not covered by CaF_2, while 3×1, and 1×3 patterns can be associated with the [110] and [1$\bar{1}$0] nanostripes.

As CaF_2 coverage approaches 1 ML, the nanostripes coalesce into a complete wetting layer and form flat terraces with rectangular edges. An example of a terminated wetting layer is shown in Fig. 2(b) where individual nanostripes (labeled *C*) can be resolved. At 1 ML of coverage the redistribution of the terraces is terminated and all the terraces consist of [110] parallel nanostripes. The wetting layer has a dominating single-axis anisotropy, which is confirmed by the 3×1 LEED single-domain pattern [inset in Fig. 2(b)]. Triple periodicity is observed in the [1$\bar{1}$0] direction that is perpendicular to the nanostripes.

Above 1 ML of coverage, the growth proceeds in three-dimensional mode. Long CaF_2 stripes ~1–3 nm in height appear at the surface [labeled *D* in Fig. 2(c)] and run parallel to the [110] direction. However, unlike the nanostripes, these stripes are not confined into a single terrace. Having length of several microns they cross many steps. Between them one can still resolve the nanostripes of the wetting layer [labeled *C* in Fig. 2(c)].

Judging solely from AFM measurements, it is difficult to resolve the exact shape of the islands because at 10 nm scale the images are noticeably influenced by the shape of the tip. To get further structural information, RHEED measurements were carried out during the three-dimensional growth. With the *e* beam perpendicular to the stripes, transmission spots originating from 3D diffraction are observed [Fig. 2(d)]. The

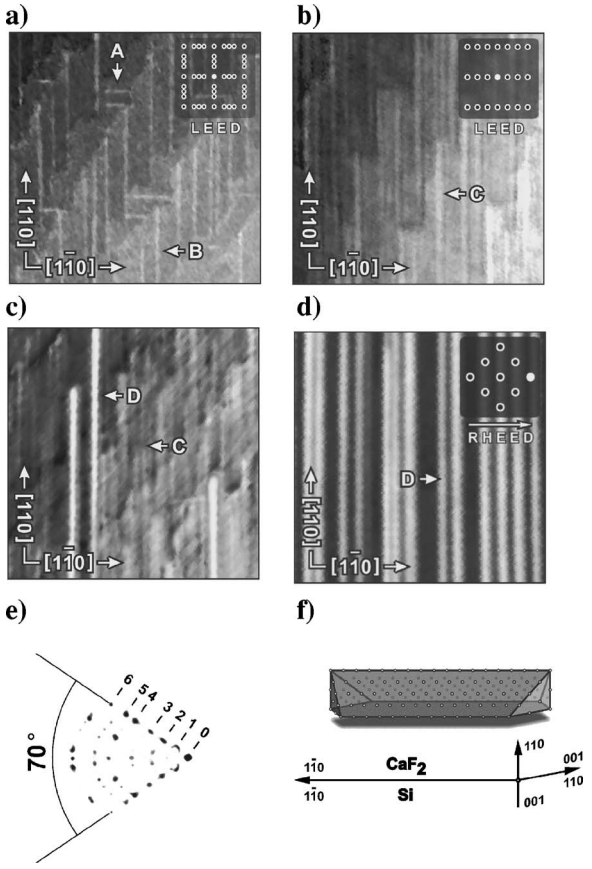

FIG. 2. High-temperature (770 °C) deposition of CaF_2. (a) 0.1 ML coverage; AFM scan dimensions 800 nm×800 nm×1.5 nm; inset: LEED shows 3×1 together with 1×3 surface reconstruction mixed with 1×2 double-domain pattern of the Si(001) surface. (b) 1 ML coverage; AFM scan dimensions 800 nm×800 nm ×1.5 nm; inset: LEED shows single domain 3×1 surface reconstruction. (c) CaF_2 ridges begin to form on top of the wetting layer at 1.1–1.2 ML coverage; AFM scan dimensions 800 nm×800 nm ×12 nm. (d) Many CaF_2 ridged islands have formed at 6 ML of coverage; AFM scan dimensions 800 nm×800 nm×12 nm; inset: RHEED with *e* beam across the ridges shows 3D transparency spots corresponding to the CaF_2 (110) lattice orientation. (e) RHEED pattern evolution with incidence angle shows inclined streaks (*e* beam along the ridges). (f) Schematic view of a ridge faceted with {111} planes.

pattern corresponds to the fcc lattice of CaF_2 being rotated with respect to the fcc lattice of Si so that the CaF_2 (110) and Si (001) planes become parallel. Within these planes the CaF_2 $[1\bar{1}0]$ direction becomes parallel to the Si $[1\bar{1}0]$ axis.

With the *e* beam parallel to the stripes surface diffraction from the stripe facets is observed. Figure 2(e) shows an overlapped stack of six RHEED patterns taken at different incidence angles. It can be seen that as the angle is varied, individual reflections (labeled 1–6) move along the streaks inclined 35° with respect to the substrate normal, corresponding to surface diffraction from the planes inclined 55° with respect to the substrate normal. Moreover, at each fixed incidence angle, RHEED spots reflecting the 3×1 periodicity appear on concentric circles. Together with the epitaxial relations derived so far, this implies that the side slopes of the stripes are formed by CaF_2 {111} planes. Taking into account the AFM data, we conclude that an individual stripe looks like an elongated hut with the roof formed by two {111} planes, each end closed by two {111} facets perpendicular to the substrate surface and making 35° with the stripe axis [Fig. 2(f)]. The results on lattice orientation and island faceting are consistent with what was observed by TEM in Ref. 13. Faceting is consistent with the fact that {111} planes in the fluorite lattice have minimal surface free energy.

These epitaxial relations are quite unusual for CaF_2 on Si. They are assumed to be induced by the interface wetting layer. According to LEED and RHEED data the wetting layer has a 3×1 superstructure. This superstructure is supposed to define the (110) orientation of the next CaF_2 planes. A possible explanation is based on the fact that a rectangular unit cell of the 3×1 surface has the size of $(3a_0/\sqrt{2}\times a_0/\sqrt{2})$, which is almost the same size as two unit cells of CaF_2 in the (110) plane $(2a_1\times a_1/\sqrt{2})$. Here by a_0 and a_1 we denote the lattice constants of Si and CaF_2, respectively ($a_0=5.43$ Å, $a_1=5.46$ Å).

Most of the 3D stripes observed by AFM are uniform in width. However, the height and width of the stripes whose up-the-steps end falls within the image bounds noticeably increase along the stripe in the down-the-steps direction, compensating for the decrease in the absolute height induced by the steps. In this respect, the stripe is roof like with the side slopes formed by step-free {111} surfaces [Fig. 2(f)]. Far from the thin end of the stripe, saturation of the width is observed, which is probably related to strain effects due to large lattice misfit across the stripe. It is likely that the stripe nucleates at its thinner end and grows preferentially in the down-the-steps direction. The further increase of the coverage leads to higher density of the stripes [Figs. 2(c) and 2(d)].

C. Low-temperature growth

As observed in preceding works,[15,16] the deposition of CaF_2 on the Si(001) surface heated to 450 °C results in the formation of almost uniformly distributed CaF_2 islands (Fig. 3) having height of 3–8 nm and lateral size below 10–20 nm. Individual islands (labeled *A*) are rectangular based and aligned with respect to the [110] and $[1\bar{1}0]$ directions of the substrate. With the increase of CaF_2 coverage the density of the nanostructures grows while their shape and size remain constant.

To get further information on the structure of the islands, RHEED patterns were recorded during growth. The inset in Fig. 3(a) shows a RHEED pattern taken with the *e* beam running along the [110] direction of the substrate. The analogous pattern taken in the perpendicular $[1\bar{1}0]$ direction (not shown) appears to be identical, indicating a fourfold symmetry of the growing structures. Transmission spots are clearly seen in the pattern, originating from 3D diffraction of the grazing incidence electron beam on the island lattice. The observed pattern corresponds to the fcc lattice of CaF_2 being oriented identically to the lattice of the underlying Si substrate. Apart from the transmission spots, the RHEED pattern

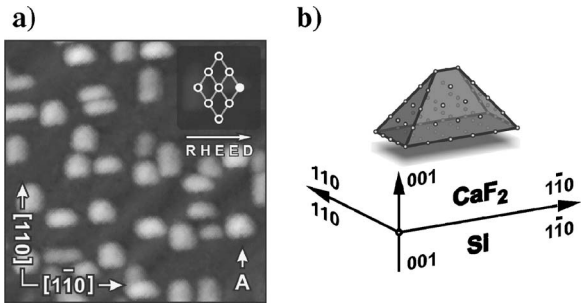

FIG. 3. Low-temperature (400 °C) deposition of CaF_2. AFM image (a) shows rectangular-based huts of almost the same size 30 nm×25 nm×6 nm (labeled *A*). In the inset a typical RHEED pattern is given with bright 3D transparency spots and inclined streaks. According to RHEED, the huts are faceted with {111} planes and have the lattice oriented in the same way as the Si substrate. In (b) a schematic view of an individual hut with {111} facets is given. AFM scan dimensions 300 nm×300 nm×8 nm.

shows streaks inclined by 55° with respect to the substrate normal that can be interpreted as 2D diffraction from two {111} planes parallel to the *e* beam and making an angle of 55° with the substrate surface plane. Putting together this observation with the AFM data available, we conclude that the islands have the shape of rectangular based huts that are faceted with four {111} planes [Fig. 3(b)].

LEED patterns (not presented) show that within the first 2–3 ML of CaF_2, the surface exhibits gradual transition from the $2\times1+1\times2$ periodicity of the clean Si to the 1×1 periodicity of the overlayer. This is in agreement with the observation[16] that at low-temperature CaF_2 does not wet the Si(001) surface and that, until coalescence of separate islands at few monolayers of coverage, silicon remains intact in the area between the islands.

IV. ELECTRONIC PROPERTIES

In correspondence with the two growth regimes (high- and low-temperature deposition), photoemission spectra were taken from the shallow core levels of the adsorbate (Ca 3*s*, Ca 3*p*, F 2*s*), from the F 2*p* valence band, from the Si 2*p*, Ca 2*p*, and F 1*s* core levels as a function of the amount of deposited material. Moreover, x-ray absorption spectra in correspondence of the Ca 2*p* edges were measured. The purpose was to focus on the chemical reactions occurring at the interface and to identify bonding configurations in the different regimes through the analysis of spectral lineshape and core level shifts.

A. High-temperature growth

1. Photoemission

In Fig. 4(a) the evolution of the shallow Ca 3*s*, F 2*s*, and Ca 3*p* core levels and F 2*p* valence band of the CaF_2/Si(001) system is shown as a function of the amount of deposited material for the samples grown at a substrate temperature of 750 °C. A photon energy of 90 eV was used. Spectra were recorded at normal emission with an angular

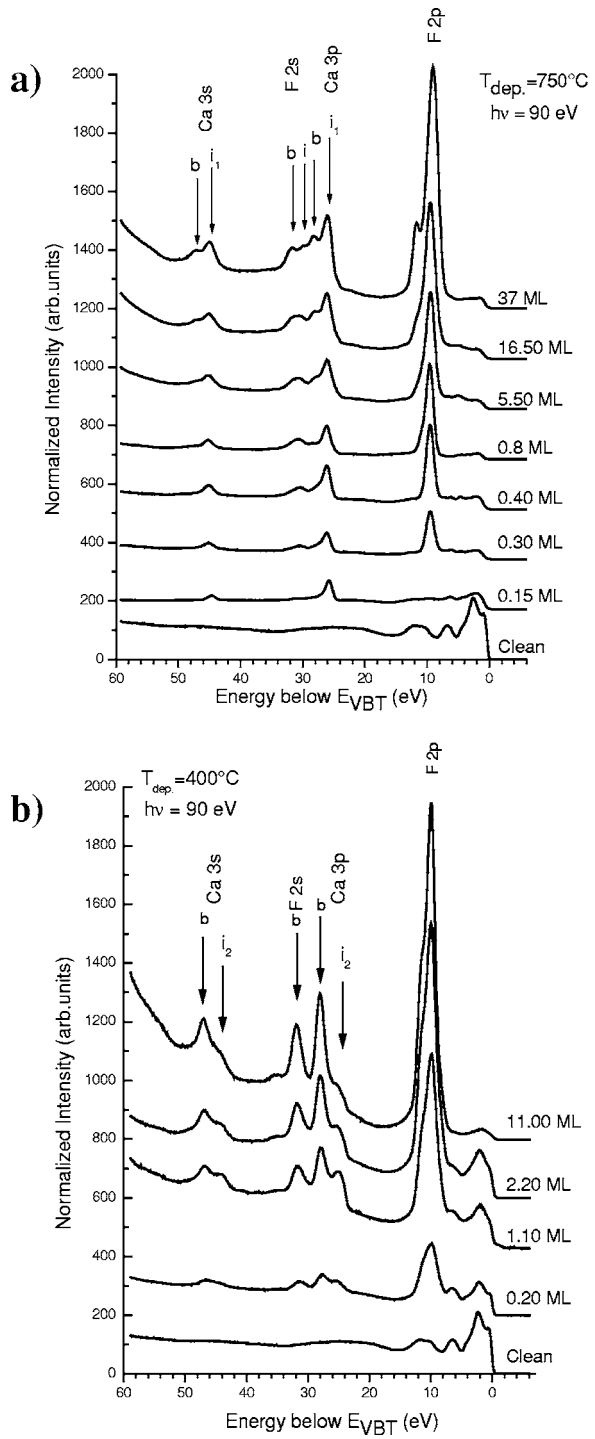

FIG. 4. Photoemission spectra taken at 90 eV photon energy at normal emission as a function of coverage at high (a) and low (b) substrate temperature during deposition. The energy scale is referred to the clean Si valence-band top. The spectra have been normalized to the incoming photon flux. The spectrum of the clean substrate is also shown for comparison.

acceptance of 2° and an overall energy resolution (photon and electron analyzer) of 0.2 eV.

The clean spectrum shows the characteristic features of Si(001). In particular the peculiar surface state of the clean Si(001) 2×1 surface is visible at about 0.7 eV of binding

TABLE I. Core-level binding energies referred to the Si valence-band top. *b* indicates bulk level values, and *i*, i_1, i_2, i_3 refer to different interface components, as shown in Figs. 4 and 6. HT refers to high-temperature growth and LT refers to low-temperature growth.

	Bulk	Ca interface components			F interface components
	b	i_1 (HT)	i_2 (LT)	i_3 (HT)	*i* (HT)
Ca 3*p*	28.2±0.2	26.1±0.2	25.3±0.2		
Ca 3*s*	47.0±0.2	45.1±0.2	44.3±0.2		
Ca $2p_{3/2}$	348.9±0.2	347.1±0.2	345.2±0.2	346.1±0.2	
F 2*s*	31.7±0.2				30.4±0.2
F 1*s*	686±1				684±1

energy.[15,16] At the earliest stages of CaF_2 deposition (0.15 ML) at high temperature, the structures of the Si substrate are severely dumped and smeared out, with the emergence of evident contributions only from Ca 3*s* and Ca 3*p* states at about 44.8±0.2 eV and 25.8±0.2 eV, respectively. It was already noted in previous works[15–17] that adsorption at high temperature is accompanied by molecular dissociation at the interface between the substrate and adsorbate. This is by the way a behavior also observed by different authors on Si(111),[9,10] where CaF was seen to form at the interface with Ca directly bonding to the substrate Si atoms. Interestingly, contributions from fluorine species seem to be absent in the present case at 0.15 ML, suggesting a complete dissociation of the molecule at very low coverage. Fluorine features show up at 0.30 ML of coverage. Both a broad structure associated to the F 2*s* states is observed at 30.4 eV and a F 2*p*–related valence band develops, centered at about 9.5 eV.

At 0.8 ML fluorine features progressively increase, and according to F 2*s* and Ca 3*p* intensities, the fluorine to Ca ratio grows up. Referring to AFM, this coverage range corresponds to the almost completion of the wetting layer. In this respect, photoemission clearly indicates that both Ca and F contribute to the formation of the wetting layer.

At higher coverage, Ca and F structures split. In particular Ca 3*s* shows two components at 47.0±0.2 and 45.1±0.2 eV, Ca 3*p* presents also two components at 28.2±0.2 and 26.1±0.2 eV, and F 2*s* shows a double peak at 31.7±0.2 and 30.4±0.2 eV. A similar trend was observed previously for CaF_2 grown on Si(111),[9,10] and split components were ascribed to bulk CaF_2 and to reacted fluoride molecules at the interface. Following the same interpretation,[17] features labeled *b* in Fig. 4(a) are referred to bulk fluorite levels due to the formation of three-dimensional islands and features labeled *i* and i_1 are associated with fluorine and calcium atoms in the interface region.

It should be noted that Ca 3*s* and 3*p* features related to interface atoms show a slight shift of 0.3 eV towards higher binding energy when passing from initial adsorption to higher coverage. This was not observed on Si(111) and can be correlated to the stronger molecular dissociation observed on Si(001) at extremely low coverage, leading to almost complete absence of F at the surface at 0.15 ML. Core-level positions and shifts are resumed in Table I.

Concerning the F 2*p* valence band, the narrow atomiclike peak broadens in a double-peaked structure. This is consistent with the development of a bulklike valence band. Again an analogous behavior was observed on Si(111).[9,10]

It can be noticed that even at the highest coverage investigated (30 ML) interface-related features dominate the spectrum. According to electron mean-free-path calculations[23] for the measured kinetic energies of the Ca and F interface peaks, they should not contribute to the spectra already at 5.5 ML, in the case of the formation of uniform and homogeneously thick fluorite layers over the substrate surface. Test AFM scans taken on these samples after completion of the photoemission measurements confirmed that the wetting layer was only partly covered by bulk islands and that very high fluoride islands were present coexisting with the wetting layer and with the 3D stripes. This type of growth was seen to occur in the presence of defects at the surface (step bunches which act as nucleation sites for the high fluoride islands). The formation of some defects at the surface could be expected in the present case due to heating of the substrate which was not optimal (in terms of temperature uniformity and heat quenching immediately after deposition) during the synchrotron runs with respect to the Ioffe growth experiments. However, we believe that this does not influence the spectral feature interpretation.

High-resolution photoemission spectra from the Si 2*p* levels taken on the clean Si(001) 2×1 surface and at low CaF_2 coverage are shown in Fig. 5. Spectra were acquired at an emission angle of 45° (8° of angular acceptance) and with a photon energy of 138 eV to enhance the surface sensitivity. The total energy resolution (photon and electron analyzer) was better than 80 meV. The spectra reported in Fig. 5 are shown after background subtraction.

The spectrum acquired on the clean surface is decomposed into components consisting of five Voigt doublets accounting for spin-orbit splitting [Fig. 5(a)]. Best fit results are obtained using a common Gaussian width of 280 meV, a Lorentian width of 85 meV, a spin-orbit splitting of 606 meV, and a branching ratio for the $2p_{1/2}$ and $2p_{3/2}$ components of 0.53. The spectrum and fit results are in agreement with the work of Landemark *et al.*[24] Following the notation of Landemark *et al.*[24] the components of the clean Si(001)-(2×1) surface are denoted by *S*, *SS*, *B*, *S'*, and *C* for dimer-up, dimer-down, bulk, second-layer, and third-layer atoms, respectively. The energy shifts of the *S*, *C*, *SS*, and *S'* doublet components with respect to the bulk component *B* are −480, −220, 80, and 340 meV. Additional step-related

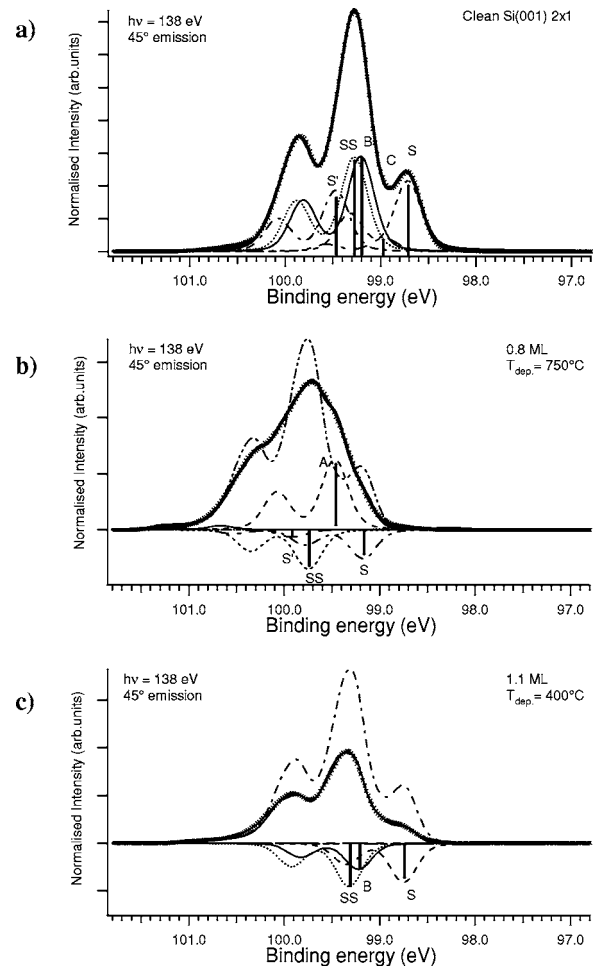

FIG. 5. Si $2p$ photoemission spectra taken (a) on the clean substrate, (b) at 0.8 ML of CaF_2 coverage at high temperature, and (c) at 1.1 ML of coverage at low temperature. Spectra have been recorded at an emission angle of 45° and at a photon energy of 138 eV. Reported spectra have been normalized to the incoming photon flux and a Shirley background subtraction was applied before display. Spectra were fitted with multiple Voigt doublet components.

components due to the use of a substrate with a miscut angle of 1–3 mrad are not discernible from our data.

In Fig. 5(b) the spectrum recorded in correspondence of the almost completed wetting layer is shown. The line shape is drastically changed with respect to the clean substrate, and the spectrum appears shifted to higher binding energy. In order to evaluate quantitatively the spectral evolution the fitting method introduced by Herrera-Gómez *et al.*[25] has been applied, according to which the spectrum of the clean surface (background subtracted) is used as a building block to fit the rest of the data. In particular the spectrum of Fig. 5(b) is fitted by using the clean spectrum curve as a fitting peak plus additional Voigt Si $2p$ doublets of the same type described above, which were allowed to be either negative or positive so that their total area was forced to be null. While a positive component represents the appearance of a new chemical component, a negative doublet represents the disappearance of a chemical component of the clean surface. The area of the clean surface curve used in the fit is kept fixed, normalized to the area of the spectrum to be fitted. This method leaves out a detailed determination of all components involved in the formation of the electron distribution curve. Especially when a spectrum consists of many shifted components [as for Si(001) 2×1], a precise identification of their evolution in the presence of an adsorbed species can be difficult: an adsorbate can induce band bending or charging effects in addition to adsorbate-induced shifted components and quenching of preexisting ones. The method used here permits to evaluate separately band bending, through the observation of the displacement of the clean surface curve, from features rising from bonding and charge transfer between substrate and adsorbate and simultaneous quenching of components associated with the unperturbed surface. Inhomogeneous band bending,[26] which is known to produce core-level broadening, shift, and line shape change on semiconductor surfaces, can induce sizable effects on the spectra at very low—submonolayer—coverage (not shown here), but should be ineffective in the present case at about 1 ML, in correspondence with the formation of the uniform wetting layer.

The result of the fit reported in Fig. 5(b) clearly shows the progressive quenching[27] of features *S*, *SS*, and *S'*, associated with the clean surface reconstruction, and the birth of a new feature (labeled *A*) displaced by 0.2 eV toward lower binding energy with respect to the bulk component. This component can be ascribed to a bonding between Si and Ca. This result is similar to what observed upon chemisorption at high temperature on Si(111), where molecular dissociation was seen to occur with the formation of a CaF molecular species bonding to Si substrate atoms through Si-Ca bonding.[9,10] The present result is also consistent with the results reported by Pi *et al.*[28] on Si(001). In that work, however, it was concluded that the terminated interface layer consisted only of Ca atoms. Photoemission from shallow core levels in the present study clearly indicates that this is not the case: F atoms also contribute to the formation of the wetting layer [Fig. 4(a)]. The discrepancy between the two results is probably related to the different deposition conditions used in Ref. 28 and in particular to the lower evaporation rates used in that study. It will be shown later on in this work that lower deposition rates result in a drastic reduction of F at the interface for comparable values of nominal thickness of deposited material.

It is noteworthy that no appreciable Si component which can be related to bonding with F is observed. In fact, bonding between Si and F atoms should induce components shifted to higher binding energy with respect to bulk levels.[9] These are negligible in the present case, indicating that bonding to the substrate in the wetting layer occurs only through Ca atoms.

The presence of only one Ca-induced component and the overall reduction of the clean surface reconstruction features seem to suggest a single type of adsorption geometry for all Ca atoms and a removal of the 2×1 asymmetric dimer reconstructed structure by the wetting layer.

Concerning the whole spectrum in Fig. 5(b), the fit indicates an overall shift with respect to the clean surface of 0.48 eV toward higher binding energy. A similar effect was also observed by Pi *et al.*[28] This displacement could be related to a band bending due to the adsorbate, even if some

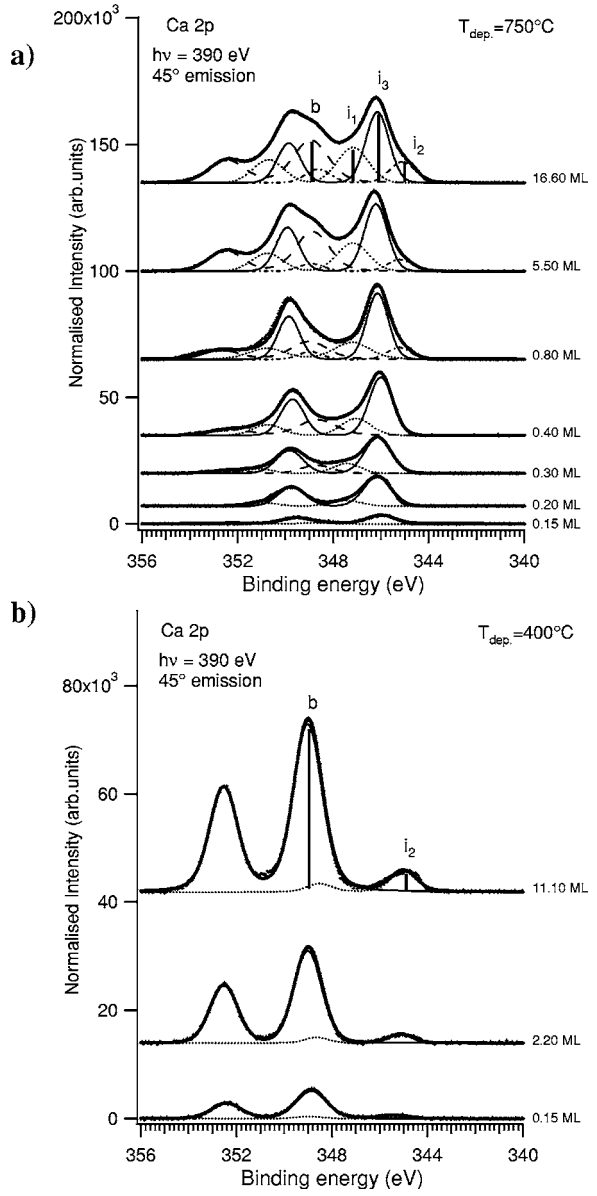

FIG. 6. Ca 2*p* photoemission spectra taken as a function of coverage at an emission angle of 45° and at a photon energy of 390 eV (a) for high-temperature and (b) low-temperature deposition. Reported spectra have been normalized to the incoming photon flux and background subtracted before display. Spectra were fitted with multiple Voigt doublets.

degree of sample charging associated with non-neutralized holes left during the photoexcitation event cannot be ruled out.

In Fig. 6(a) the evolution of the Ca 2*p* core levels is reported. Spectra were acquired at an emission angle of 45° (8° of angular acceptance) and with a photon energy of 390 eV. The overall energy resolution was 0.2 eV. In order to achieve more quantitative chemical information, the spectra are decomposed into a sum of Voigt doublets, taking into account a $2p_{1/2}$-$2p_{3/2}$ spin-orbit splitting of 3.6 eV.

Since the initial adsorption stages, best fits to Ca spectra are obtained with two doublet components at 347.1±0.2 and at 346.1±0.2 eV (Ca $2p_{3/2}$), labeled i_1 and i_3, respectively, in Fig. 6(a) and in Table I. Their intensity progressively increases with thickness, with their branching ratio (i_3/i_1) passing from 7 at 0.15 ML to about 2 in correspondence with the completion of the wetting layer (0.8 ML), then stabilizing for higher coverage. These two features are both associated with the formation of the wetting layer. Feature i_1 in particular is in good agreement with the interface-related component observed for CaF_2 on Si(111) (Refs. 9 and 12) and associated with the Ca-F complex. Taking into account the differences in chemisorption on the two substrates and in particular considering that in the earliest stages of wetting layer formation molecular dissociation leads to a Ca-rich surface, with negligible F contributions [as observed in Fig. 4(a)], we associate component i_3 with completely dissociated Ca atoms bonded to silicon.

On the basis of this assignment, the wetting layer would be formed at the first stage only by chemisorbed Ca atoms; it would be completed in a second step by Ca-F complexes, as on Si(111). The intensity ratio between the two components after completion of the wetting layer suggests that 2/3 of the Ca atoms in the wetting layer are bonded only to Si and 1/3 also to F atoms.

By increasing the amount of deposited material, a new component shows up at 348.9±0.2 eV, which significantly increases at high coverage, above the completion of the wetting layer. This has been labeled *b*, and it is associated with Ca atoms in a bulklike environment.[9,10,12] The appearance of the bulk component is correlated with the formation of the three-dimensional islands on top of the wetting layer. The appearance of bulk-related features even at submonolayer coverage can be explained in terms of some degree of nonideal growth, which is the development of 3D islands before the completion of the wetting layer. Another feature, which was not observed in previous studies, shows up at 345.2±0.2 eV (labeled i_2) at high coverage. The appearance of this feature in coincidence with the bulk related one suggests associating it with the development of the 3D islands as well. A precise assignment is although not straightforward. This will be addressed with more detail later in this work. However, it should be stressed that an analogous feature is also observed in Fig. 6(b), in correspondence with low-temperature growth.

F 1*s* levels were also measured at 735 eV of photon energy as a function of coverage (Fig. 7). At high-temperature deposition the wetting layer presents a single F 1*s* component at 684±1 eV. This is consistent with the results obtained on Si(111),[9,12] and the structure is associated with F atoms bonded to Ca in a Ca-F complex at the interface, after partial molecular dissociation (it has been labeled *i* in Fig. 7 and in Table I). Consistent with the other photoemission results reported in this work, no emission from F 1*s* levels is recorded at extremely low coverage below 0.2 ML, where only contributions from Ca atoms are measured.

After the completion of the wetting layer (above 1 ML) a F 1*s* bulk component shows up at 686±1 eV (labeled *b*), quickly increasing and becoming the prevailing structure for higher coverages. This is associated to the developing of the CaF_2 islands.

2. Role of evaporation rate

It was anticipated that the CaF_2 evaporation rate plays a crucial role in the determination of the surface composition,

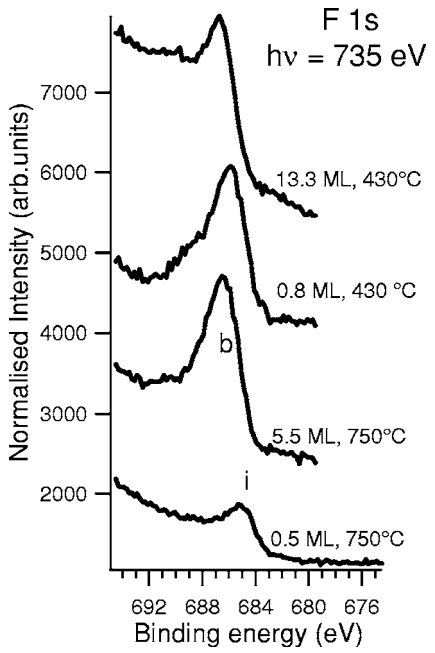

FIG. 7. Photoemission from F 1*s* core levels at different temperatures and coverage. A photon energy of 735 eV was used.

when growth proceeds at high temperature. In Fig. 8 we report spectra from the valence band and from the shallow core levels taken from samples prepared with a reduced deposition rate of 0.08 ML per min. The spectra are angle integrated and are acquired at 90 eV of photon energy in a separate run, with a double-pass cylindrical mirror analyzer.

It can be seen clearly that Ca structures dominate the spectra up to 0.8 ML of coverage. F-related features are absent and appear only in the spectrum at 1.5 ML. This result is in agreement with those reported by Pi *et al.*[28] Ca 3*p* and Ca 3*s* features are shifted to lower binding energy at low coverage with respect to their bulk position. Consistently with the results presented above, they have been labeled i_1 to indicate that they are associated to Ca atoms in the reacted interface

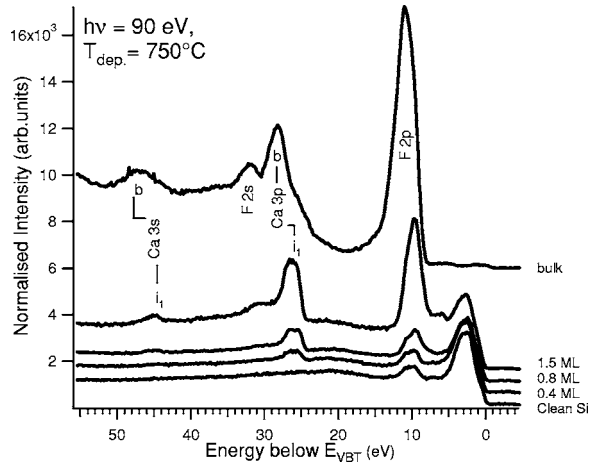

FIG. 8. Photoemission spectra taken at 90 eV photon energy at normal emission as a function of coverage at high substrate temperature during deposition with an evaporation rate of 0.08 ML per minute.

layer. Apparently, lower evaporation rates increase the degree of complete molecular dissociation at elevated temperatures at the interface. This point will be discussed later in Sec. V.

3. X-ray absorption at Ca 2p edges

In order to get further information into the details of interface formation at high-temperature deposition, x-ray absorption spectra at the Ca 2*p* edge were taken. Near-edge x-ray absorption fine structure (NEXAFS) represents a powerful tool to probe the local density of empty antibonding states, which are available for core-excited electrons of the absorbing element. In particular, for the $L_{2,3}$ edges the spectral line shape can be correlated to the oxidation state or valence of the absorbing atom.[29] Unoccupied states can be monitored at the absorption site, and this is particularly useful when the adsorbing species are located at an interface between different materials.

Ca 2*p* absorption spectra are mainly determined by the transition from 2*p* core levels to the empty localized 3*d* states. The fine structure of the Ca 2*p* soft x-ray absorption edge was studied in detail by Himpsel *et al.* both experimentally and theoretically.[29] In Fig. 9 we present x-ray absorption spectra taken as a function of coverage of CaF_2 on Si(001) for two different evaporation rates [2 ML per minute in Fig. 9(a) and 0.08 ML per minute in Fig. 9(b)]. The spectrum acquired at 6 ML deposited onto Si(111) at 730 °C is also shown for comparison in Fig. 9(c). Data were taken in *s*-type light polarization conditions at an incidence angle of 70°. The spectra were normalized to the incident photon flux.

Absorption spectra are characterized by two prominent features due to transitions to 3*d* levels from spin-orbit split $2p_{3/2}$ and $2p_{1/2}$ core states. A number of smaller features are also present, their number and intensity strongly depending on the atomic chemical oxidation state, atomic geometry, and coordination with neighboring atoms. They originate from mixing of states due to interaction of the core hole with the valence electrons and crystal field effects.

From Figs. 9(a)–9(c) it is evident that the different deposition conditions influence the line shape, especially at low coverage. The spectrum taken at 6 ML of CaF_2 on Si(111) is in perfect agreement with the results reported by Himpsel *et al.*[9,29] for the same system. The multiplet split structure in Fig. 9(c) can be correlated to Ca atoms in a 2+ oxidation state within the CaF_2 lattice. It is well known that the growth mode on Si(111) proceeds in a layer-by-layer form.[9–12] Only the first interface layer is characterized by molecular dissociation with a change in bonding and valence of the Ca atoms, which form Si-Ca-F complexes. Six monolayers are sufficient for the Ca edges to present the typical eightfold coordination line shape of bulk CaF_2.[29]

Spectra taken at submonolayer coverage on Si(001) are instead characterized by almost negligible multiplet fine structure. In both Figs. 9(a) and 9(b), spectra present asymmetric spin-orbit split doublet lines. Interestingly, the asymmetry is reversed in the two cases: high evaporation rate results in asymmetric Ca 2*p* edges toward the lower photon energies, while low evaporation rate results in an asymmetry toward the higher binding energies. The spectra in Fig. 9(a)

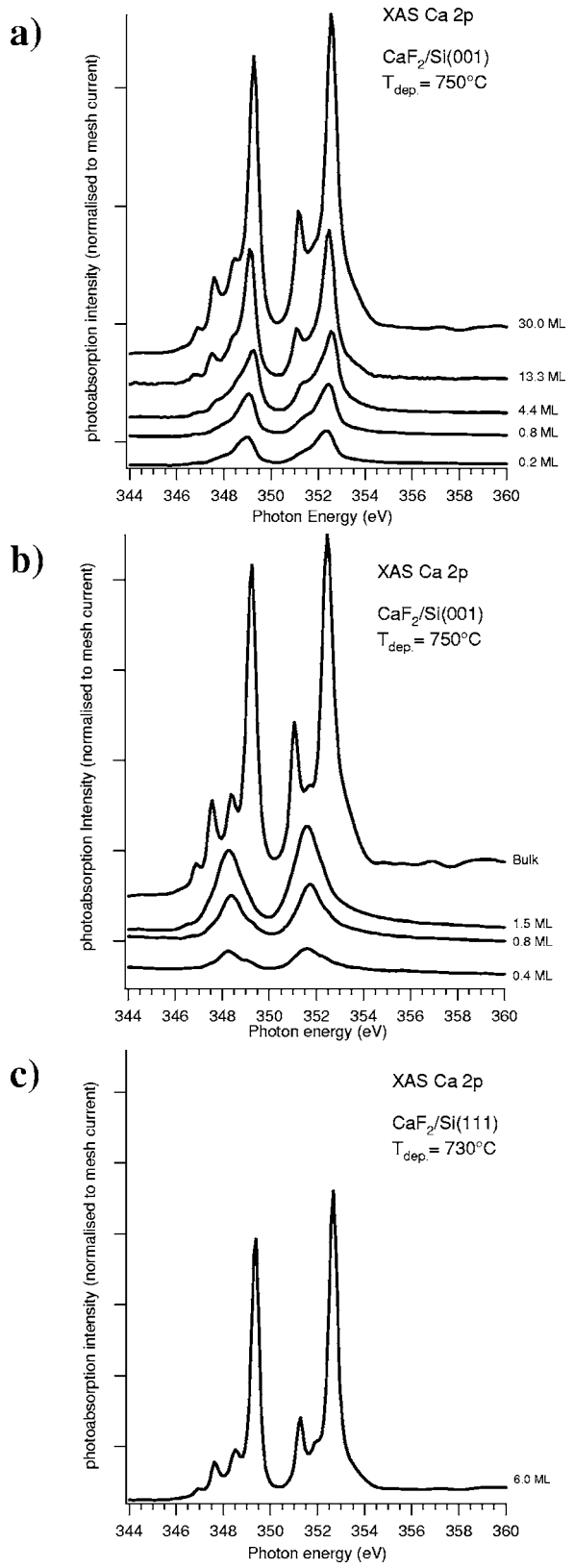

FIG. 9. X-ray absorption spectra taken as a function of coverage at Ca 2*p* edges on samples grown at high temperature: (a) high deposition rate and (b) low deposition rate. (c) refers to deposition on Si(111).

can be correlated with those reported in Ref. 29 for 1 ML of $CaF_2/Si(111)$. A similar line shape was interpreted there in terms of the variation of Ca oxidation state at the interface, passing from 2+ to 1+, and it was associated with Ca atoms in the Si-Ca-F complex. This picture is consistent with the data presented so far on Si(001), where dissociation of the CaF_2 molecules is seen to occur in the wetting layer. The small differences with respect to the spectrum of 1 ML of $CaF_2/Si(111)$ (Ref. 29) can be ascribed to the superposition with the signal from Ca atoms bonding to Si from completely dissociated molecules. This is more evident in Fig. 9(b), where the line shape at monolayer and submonolayer coverage is in good agreement with that expected for metallic Ca or Ca bonded to Si at a Ca/Si interface.[29] We take this as further evidence of complete dissociation of the molecule at the initial stages of wetting layer formation, with the evaporation of F in volatile compounds with Si and direct bonding between Ca and Si. This process is emphasized if deposition is carried out at low evaporation rates.

B. Low-temperature growth

1. Photoemission

The evolution of the shallow core levels when deposition is carried out with the substrate held at 400 °C is shown in Fig. 4(b). It can be noticed that since the earliest deposition stages, structures associated with Ca 3*s* and 3*p* and F 2*s* bulk levels (labeled *b*) give the most intense signals. Silicon valence-band structures below 4 eV of binding energy are evident up to 2.2 ML, and the characteristic surface state of Si(001) 2×1 can still be observed at 0.2 ML of coverage, indicating that part of the substrate surface is still uncovered by CaF_2. This was also noticed by using He I photoemission, as reported elsewhere.[15]

Interestingly, Ca 3*s* and 3*p* levels show additional split structures at 44.3 ± 0.2 and 25.3 ± 0.2 eV, respectively. These have been labeled i_2 and, in analogy with the high-temperature growth case, they can be associated with Ca atoms at the buried interface. We associate these features with buried interface atoms because no wetting layer is observed to form by AFM, RHEED, and LEED at low temperature and the surface portion not covered by CaF_2 islands was seen to remain clean Si. Furthermore, He metastable deexcitation data[15,16] seem to exclude the presence of Ca atoms at the external facets of the pyramidal islands, which on the contrary appear to be fluorine terminated. It should also be stressed that these Ca interface features are shifted by about 3 eV to lower binding energy with respect to their associated bulk structures, exceeding by 1 eV the shift observed in the case of high-temperature growth.

With reference to the F 2*p* valence band, differences with respect to the high-temperature growth are clearly evident. In particular, since the earliest deposition stages, a broad structure is present, centered at about 10 eV of binding energy. This is consistent with the formation of a bulklike valence band. Differences in line shape with respect to high-temperature growth should be associated with the different shapes and dimensions of the islands formed at the surface in the two situations.

Concerning Si 2*p* levels, Fig. 5(c) shows the spectrum obtained at 1 ML of CaF_2 coverage. The same fitting procedure used for the high-temperature sample was applied. It can be immediately seen that no sizable shift of the overall features with respect to the clean spectrum is present. Furthermore, no new features associated with charge transfer and bonding between substrate and adsorbate atoms show up. Only a progressive decrease of the most intense spectral components *S*, *SS*, and *B* associated with the clean surface is observed. This is consistent with the formation of CaF_2 islands which partly mask clean surface areas (as observed by AFM).

In Fig. 6(b) the evolution of the Ca 2*p* levels is reported. While feature labeled by *b* is the dominating one and is associated with Ca in bulk CaF_2 environment, another minor feature, labeled i_2, is always present in the spectra. It can be well noted that feature i_2 is present since the earliest stages of deposition and progressively increases with the increasing of feature *b*. The intensity ratio between the two components is about 0.1, and it appears to be independent of coverage. It should be noted that features i_2 both in Ca 2*p* [Fig. 6(b)] and Ca 3*p* [Fig. 4(b)] spectra show unusually large shifts with respect to the related bulk-level position. These originate from the same type of Ca atoms in the growing system. From structural and morphological investigation and photoemission results reported so far, component i_2 does not seem to be associated with single metallic Ca atoms bonded to Si substrate atoms nor to Ca atoms on the facet surfaces of the CaF_2 islands (these appear to be F terminated[15]). One possibility is associating it to Ca atoms at the buried interface between the CaF_2 islands and the substrate. The reason of the large binding energy shift with respect to the bulk component is although unclear. Core level shifts are determined by different factors: initial state effects (charge transfer due to chemical reactions, Madelung electrostatic potential for ionic insulators) and final state effects (relaxation of the solid electronic orbitals after the creation of the core hole, polarization response of the neighboring atoms). The different factors can act in opposite directions, partially compensating each other, or adding accordingly, making evaluations on the nature of the core-level shift sometimes difficult to achieve. It was shown by Rotenberg *et al.*[12] by using an electrostatic model that good estimates of the overall core-level shifts can be obtained if both initial- and final-state effects are taken into account and in particular it was observed that the electrostatic Madelung potential at the core hole and the polarization response of the insulator at the core hole played the major role in the determination of Ca 2*p* core-level shift for the CaF_2/Si(111) system. A dedicated calculation is beyond the aim of the present work. We believe this experimental observation will stimulate further experimental and theoretical investigations of the nature of the shifted feature i_2.

Another possibility is to associate feature i_2 with the presence of metallic Ca clusters or to the removal of the topmost fluorine layer at CaF_2 island facets thus leading to Ca-terminated surfaces, induced by interaction with the synchrotron light. Damaging effects on CaF_2 due to irradiation and leading to a fluorine depletion at the surface have been reported so far by different authors.[30,31] A binding energy shift of 3.8 eV was also reported by Himpsel *et al.*,[29] but the spectrum was not shown. Spectra reported in Fig. 6 were acquired at an insertion device beamline, with a photon flux lower than 10^{12} photons/s, which is well below the value reported in Ref. 30 for the saturation of the surface dissociation effects. In particular we did not notice any appreciable spectral evolution of the i_2 feature (e.g., we did not notice any increase) upon multiple scans in the Ca 2*p* region. In a separate synchrotron run, lower photon fluxes from a bending magnet were used (of the order of 10^{10} photons/s), but the feature i_2 was always present and it did not change its intensity after multiple scans. For this reason the interpretation of feature i_2 in terms of irradiation effects seems unlikely. Finally we tend to exclude that component i_2 is caused by some degree of oxygen contamination, since no characteristic feature is observed in the valence band region at 5–6 eV of binding energy [Fig. 4(b)].

Concerning the F 1*s* level, at low temperature only one component is present associated with bulk calcium fluoride (labeled *b* in Fig. 7) at all coverages, consistent with the formation of three-dimensional islands since the earliest deposition stages.

V. DISCUSSION

The data presented in this work clearly point out two main and distinct growth modes for CaF_2 on Si(001) which depend on the substrate temperature during deposition. In both cases the growth results in the formation of nanodimensional islands, which are pyramidal in shape for growth temperatures below 600 °C (Volmer-Weber type of growth) and elongated stripes on top of a reacted uniform fluoride layer for growth temperatures above 600 °C (Stranski-Krastanov type of growth).

Growth at high temperature indeed represents the most interesting case: first because sufficiently thick layers give rise to almost uniformly grooved and ridged surfaces, generated by the coalescence of neighboring parallel CaF_2 stripes. These ridged surfaces can be used as a buffer layer for the subsequent growth of different materials: e.g., multilayer stacks, patterned materials in the form of parallel wires guided by the grooves, like strings of magnetic nanoclusters or organic molecules[32] attached to CaF_2, commensurate crystalline oxides on Si(001).[33] Second, the chemical reactions occurring at the interface determine the geometry of the wetting layer, which in turn drives the unusual orientation of CaF_2 crystal onto Si(001).

Therefore, understanding the details of wetting layer formation, including adsorption sites and atomic geometry, appears as a crucial point both for fundamental and technological reasons. With this respect, a key aspect is represented by the mechanisms which determine molecular dissociation and subsequent formation of the reacted nanostripes giving rise to the wetting layer.

Spectroscopic data suggest that when CaF_2 molecules are adsorbed at high temperature Ca atoms are reduced to the Ca^+ or Ca^0 valence states and F is removed from the surface. Moreover, Si terraces are seen to be consumed selectively (*B*-type terraces increase at the expense of *A*-type terraces). The etching of Si(001) surface by CaF_2 molecules may occur in accordance with the following reactions:

$$2CaF_2 + Si \rightarrow 2(CaF)_{ad} + SiF_2, \quad (1)$$

$$CaF_2 + Si \rightarrow Ca_{ad} + SiF_2, \quad (2)$$

$$2CaF_2 + Si \rightarrow 2Ca_{ad} + SiF_4. \quad (3)$$

In these reactions, SiF_4 and SiF_2 represent volatile species which can leave the surface.[34] Photoemission data presented in Sec. IV show that at $T=750$ °C and very low deposition rate (0.08 ML per min) complete reduction of Ca occurs, in agreement with reactions (2) and (3). Since reaction (2) is known to require a temperature above 1000 °C, reaction (3) is the most probable one to take place in the present case. The reduced Ca interacts with Si surface atoms and forms a silicide layer, preventing further etching of silicon.

For a Si atom on a reconstructed vicinal Si(001) surface there are different types of dangling bonds [refer to Fig. 1(b)]: two of them correspond to the empty and filled two-electron bonds of the asymmetric dimers.[22] The other one corresponds to the electronic states of the atoms located at the $\langle 110 \rangle$ steps which are perpendicular to the dimer rows within the upper terrace [terrace *A* in Fig. 1(b)]. These Si radicals should be the most active participants in the CaF_2 depletion reaction. In the general case of step edges not parallel to the [110] or $[1\bar{1}0]$ directions, each step edge would consist of longer [110] sections and shorter $[1\bar{1}0]$ sections (note that [110] was defined earlier as the $\langle 110 \rangle$ direction making less than 45° with the step edges). It is noteworthy that downward steps of type-*A* terraces will contain more Si radicals per unit length with respect to type-*B* terraces.

Inspection of Fig. 2(a) reveals that each nanostripe is confined within a single terrace and terminates at its step edges. While the down-the-steps end of the nanostripe does not seem to produce perturbation to the down-the-steps terrace edge, in correspondence with the up-the-steps end a substantial consumption of Si atoms from the upper terrace is observed. As a consequence, the nanostripe develops in the region previously occupied by the Si upper terrace. To explain this we suggest that dissociation of CaF_2 molecules takes place at the step sites where the radical type of Si atoms are located. As a result of this dissociation, fluorine atoms will form volatile molecules with Si step edge atoms, which will leave the surface and reduce the upper terrace width. Correspondingly, the lower terrace will expand. Upon dissociation the adsorbed reacted products are highly mobile at the surface at high temperature, probably diffusing preferentially along dimer rows as other alkaline-earth metals.[35] Because of their reciprocal interaction, they organize in the form of thin nanostripes on the terrace where dissociation took place.

As seen from Figs. 2(a) and 2(b), [110]-aligned nanostripes prevail at the surface, their domination becoming more evident as the coverage increases. This can be explained suggesting that the nanostripes preferentially nucleate at the downward steps of type-*A* terraces, where the density of sites for CaF_2 molecules dissociation is higher with respect to type-*B* terraces. For the same reason type-*A* terraces are consumed much faster than type-*B* terraces. This accounts for the transformation of the (2×1) double domain of the clean Si(001) surface into a single domain where terraces are separated by steps of sawlike shape with orthogonal edges and which correspond to a double atomic layer of the Si substrate.

As evidenced by photoemission and x-ray absorption, the development of the nanostripes causes a loss of the dimer pattern reconstruction, with the formation of bonding between Si and Ca atoms. By the way, the effect of the dimer pattern disruption upon molecular adsorption at temperatures above 600 °C is not unexpected and it has been observed in many other cases on Si(001).[36] Si $2p$ photoemission spectra presented in Fig. 5(b) show that at high temperature of deposition the components due to the surface reconstruction disappear. Both asymmetric dimer up and down contributions (*S* and *SS*) of the clean substrate are quenched.

Instead, a new surface component slightly shifted to lower binding energy relative to the bulk one shows up and it is associated with Si-Ca bonding. F does not seem to participate in the bonding with the substrate, similarly to the Si(111) case.[10] The binding energy shift of Si $2p$ for the Ca-Si bond in the wetting layer is small compared to that reported[37] for Ca on Si (1.0–1.35 eV), suggesting a smaller charge transfer from Ca to Si in our case. In this respect, the bonding appears more covalent. Such bonds can be formed in two ways: (i) on the basis of sp^3 hybridization, resulting in bridge-type chemisorption positions for the Ca atoms (between two Si atoms); (ii) via d^3s orbitals directed along space diagonals of a cube with the Ca atom in the center; this implies a fourfold coordination for the Ca atoms (interstitial position).

Thus two types of Ca atoms can in principle be expected on the silicon surface. While in neutral Ca the $4p$ level is the closest in energy to the $4s$ level, in Ca^+ ions the $3d$ level becomes closer to $4s$. For partially polarized Ca atoms bonding to more electronegative Si atoms ($Ca^{+\delta}$—$Si^{-\delta}$) the energies of the hybrid sp^3 and d^3s configurations on the Si surface may turn out to be very close, at least within the experimental resolution.

On the other hand, Ca $2p$ levels reveal two shifted interface components, possibly indicating two types of Ca atoms at the interface. Based on a comparison with the chemisorption of CaF_2 on Si(111),[9,12] on the sequence with which the two components appear in Fig. 6(a) as a function of coverage and on the initial depletion of F at the interface, one main component, at lower binding energy, could be associated with Ca atoms from completely dissociated CaF_2 molecules, the other with partially dissociated molecules (CaF-type complexes). The intensity ratio between the two features seems to indicate that the wetting layer is built up with 2/3 of Ca atoms of the first type and 1/3 of the second type. LEED data indicate that these are organized to built up a 3×1 periodicity with respect to the Si substrate.

The developing of the wetting layer depends not only on the substrate temperature but also on the deposition rate. It is seen that reduced deposition rates of the order of 0.1 ML per minute give rise to Ca rich films, with negligible contributions from F up to 1 ML of nominal coverage. On the other hand, a higher deposition rate (2 ML per minute) results in a 1-ML film where both contributions from Ca and F can be recorded.

A possible explanation is that F incorporation into the interface layer is a nonequilibrium process. At sufficiently low deposition rate all F evaporates in volatile compounds with Si while at higher rates some F remains at the surface bonded to Ca in analogy to the case of CaF_2 on Si(111), with the formation of Si-Ca-F complexes. This extra F is either frozen when deposition stops and the sample is cooled down or at higher coverage it becomes buried under oncoming CaF_2 (110) layers. Comparing results for different deposition rates one should also take into account that at a reduced rate the actual amount of deposited material may come out to be considerably less than estimated because of reevaporation of CaF_2 molecules from the surface at elevated temperature.[38]

As a further remark, it is useful to compare the present results with data available on simpler systems—that is, alkaline-earth metal interfaces with Si(001). Sr adsorption on Si(001) was studied by photoemission,[25] LEED,[39] and STM.[40] Ba adsorption was studied by LEED, Auger spectroscopy,[41] STM,[42] and x-ray standing-wave spectroscopy.[43] Mg adsorption was investigated by LEED and STM,[44] K and Cs adsorbtion by surface x-ray diffraction.[45] In general, the chemisorption of alkaline-earth metals on Si(001) gives rise to several types of reconstruction patterns depending on coverage and post-deposition annealing at high temperatures. For all the above-mentioned systems, stable 2×3 and 1×3 phases have been observed at the surface. However, there is not a general consensus regarding the precise adsorption sites. While several authors claim that the most favorable adsorption site is the fourfold hollow site in the through area in between the dimer rows,[43,46] others indicate the adsorption site in the valley bridge site between the dimers[40,44] or the metal atoms replacing the Si dimers.[42] Interestingly, the $3\times$ periodicity was always seen to develop parallel to the dimer row direction at a given terrace. On the contrary, the present results seem to indicate that the unit cell is rotated by 90°; that is, the $3\times$ periodicity is perpendicular to the dimer row direction on each terrace. This favors the growth of the elongated nanostripes forming the wetting layer parallel to the dimer rows. The reason of this difference could be related to the presence of the F atoms at the interface and to the role played by the Si step edges in CaF_2 molecular dissociation and in guiding the initial adsorption.

The present data do not allow us to be conclusive about the exact adsorption sites and atomic geometry. However, they give important information on surface composition, chemical reactions, surface periodicity, and orientation. We hope these results will stimulate further experiments as well as theoretical investigations. In particular, focused STM experiments would be highly desirable to unravel the questions remaining opened regarding the formation of the interface at high temperature.

After the completion of the surface reaction with the reduction of Ca and the formation of a silicide surface layer, 3D CaF_2 islands nucleate. These islands have their {110} planes parallel to Si(001). This may stabilize the 3×1 superstructure of the silicide layer. The relatively small (0.6%) misfit between the Si and CaF_2 cell along the Si ⟨110⟩ and CaF_2 ⟨100⟩ directions may facilitate this process. The more favorable epitaxial relations—that is, $Si(001)\|CaF_2(001)$—cannot be realized because Ca atoms belonging to the silicide layer have a small effective charge and for this reason they cannot coordinate efficiently with F^- in the CaF_2 (001) plane. In this case, the coordination with the electrically neutral CaF_2 (110) plane appears to be energetically more favorable.

Below 600 °C the dissociative reaction between CaF_2 molecules and Si is not activated; however, the interaction between CaF_2 and Si at the interface drives the growth of the hutlike islands. The fluoride islands grow in fact with their (001) planes parallel to the Si surface and are faceted with (111) planes which is favorable from the point of view of the free surface energy in a fluorite lattice. Furthermore, RHEED data indicate that each CaF_2 island is fully coordinated in lattice with the other islands and with the Si substrate.

The portrait of the CaF_2/Si(001) electronic interaction at low temperature is given by photoemission, showing an unexpectedly large shift of the interface Ca $2p$ levels to lower binding energies. This shift indicates a considerable decrease of the effective positive charge on the interface Ca, which can be due to the overlapping of a dangling bond of the surface Si atom with an empty orbital of Ca^{2+} (sp^3 if Ca occupies a bridge site or d^3s if Ca is at a hole site). One can expect that the role played by the d^3s orbitals in low-temperature deposition is even more important than at high temperature, because the positive charge on Ca is considerably higher in the former case. This implies a rigid shift of the CaF_2 lattice with respect to that of Si along the ⟨010⟩ direction in the ⟨001⟩ interface plane. Even in this case a full calculation taking into account both initial- and final-state effects in the photoexcitation process is highly desirable to understand more clearly the nature of the observed core-level shifts.

VI. CONCLUSIONS

The growth of CaF_2 on Si(001) 2×1 surfaces is studied following a multitechnique approach both to understand morphology and structure variations of the growing films as a function of the substrate temperature during deposition and to correlate them with electronic properties and temperature-activated chemical reactions. Structural and topographical characterization is carried out by AFM, LEED, and RHEED; electronic and chemical properties are studied by high-resolution core-level photoemission, with the analysis of core level shifts of all species (Si, F, and Ca) involved in the formation of the films, and from NEXAFS spectroscopy.

Two main growth regimes are identified. At temperatures of 400–500 °C growth proceeds in a Volmer-Weber mode with the formation of hutlike, rectangular-based, three-dimensional CaF_2 islands on top of the Si surface. CaF_2 crystal is seen to be oriented in the same way as the silicon substrate. No chemical reaction inducing molecular dissociation is observed between CaF_2 and Si. In the surface region not covered by the CaF_2 islands, the clean Si(001) 2×1 surface is seen to be preserved. At temperatures above 700 °C, growth proceeds in a Stranski-Krastanov mode with the formation of elongated, wirelike, CaF_2 islands on top of a 1-ML-thick silicide wetting layer. In particular, molecular

dissociation is seen to occur at the interface, with the consumption of Si atoms from the surface step edges. This leads to the formation of single-molecule-thick nanostripes, which coalesce into a uniform wetting layer at about 1 ML of coverage. The wetting layer has a 3×1 periodicity, which drives the subsequent orientation of the CaF_2 islands developing on its top. The proper choice of Si(001) vicinal surface permits to pass from the double-domain reconstruction typical of Si(001) 2×1 to a single-domain surface. This is due to the preferential consumption of the terraces with one of the two domains, depending on the direction of the dimer rows on that domain with respect to the step edge directions. Chemical reactions in the wetting layer involve bonding between Si and Ca atoms of the dissociated molecules. Both atomic Ca and CaF complexes are seen to form upon molecular dissociation and reaction with the substrate. Both these species give rise to the wetting layer. In particular, the Ca atoms bonding with Si are believed to determine the initial chemisorption structure of the wetting layer with 3×1 periodicity.

ACKNOWLEDGMENTS

This work has been supported by the Russian Foundation for Basic Research (Grant Nos. 02-02-17588 and 03-02-17637), the Russian Ministry of Science, an Individual International Mobility Scholarship provided by AREA (Trieste) under research project No. 4, N188, and by the Italian Ministry of Foreign Affairs, Direzione Generale per la Promozione e la Cooperazione Culturale. The experiments at the VUV and BEAR beam lines of ELETTRA synchrotron facility have been carried out along Project Nos. 2001395 and 2002507 correspondingly. The authors of the paper are grateful to the staff of these beamlines for assistance during the measurements.

[1] N. S. Sokolov and S. M. Suturin, Appl. Surf. Sci. **175–176**, 619 (2001).
[2] J. Nogami, B. Z. Liu, M. V. Katkov, C. Ohbuchi, and N. O. Birge, Phys. Rev. B **63**, 233305 (2001).
[3] A. Travos, N. Salamoura, and E. Flouda, Surf. Sci. **120**, 355 (1997).
[4] M. A. Olmstead, in *Thin Films: Heteroepitaxial Systems*, edited by W. K. Liu and M. B. Santos (World Scientific, Singapore, 1999).
[5] T. Suemasu, M. Watanabe, J. Suzuki, Y. Kohono, M. Asada, and N. Suzuki, Jpn. J. Appl. Phys., Part 1 **33**, 57 (1994).
[6] N. S. Sokolov, S. V. Gastev, A. Yu. Khilko, R. N. Kyutt, S. M. Suturin, and M. V. Zamoryanskaya, J. Cryst. Growth **201/202**, 1053 (1999).
[7] N. S. Sokolov, J. C. Alvarez, and N. L. Yakovlev, Appl. Surf. Sci. **60–61**, 421 (1992).
[8] T. Chatterjee, P. J. McCann, X. M. Fang, and M. B. Johnson, J. Vac. Sci. Technol. B **16**, 1463 (1998).
[9] D. Rieger, F. J. Himpsel, U. O. Karlsson, F. R. McFeely, J. F. Morar, and J. A. Yarmoff, Phys. Rev. B **34**, 7295 (1986).
[10] M. A. Olmstead, R. I. G. Uhrberg, R. D. Bringhans, and R. Z. Bachrach, Phys. Rev. B **35**, 7526 (1987).
[11] R. M. Tromp and M. C. Reuter, Phys. Rev. Lett. **61**, 1756 (1988).
[12] E. Rotenberg, J. D. Denlinger, M. Leskovar, U. Hessinger, and M. A. Olmstead, Phys. Rev. B **50**, 11052 (1994).
[13] D. Loretto, F. M. Ross, and C. A. Lucas, Appl. Phys. Lett. **68**, 2363 (1996).
[14] T. Sumiya, T. Miura, H. Fujinuma, and S. Tanaka, Surf. Sci. **376**, 192 (1996).
[15] L. Pasquali, S. D'Addato, G. Selvaggi, S. Nannarone, N. S. Sokolov, S. M. Suturin, and H. Zogg, Nanotechnology **12**, 403 (2001).
[16] L. Pasquali, S. Suturin, N. Sokolov, G. Selvaggi, S. D'Addato, and S. Nannarone, Nucl. Instrum. Methods Phys. Res. B **193**, 474 (2002).
[17] N. S. Sokolov, S. M. Suturin, V. P. Ulin, L. Pasquali, G. Selvaggi, and S. Nannarone, Appl. Surf. Sci. **234**, 480 (2004).
[18] C. Quaresima, C. Ottaviani, M. Matteucci, C. Crotti, A. Antonini, M. Capozi, S. Rinaldi, M. Luce, P. Perfetti, K. C. Prince, C. Astaldi, M. Zacchigna, L. Romanzin, and A. Savoia, Nucl. Instrum. Methods Phys. Res. A **364**, 374 (1995).
[19] S. Nannarone, F. Borgatti, A. DeLuisa, B. P. Doyle, G. C. Gazzadi, A. Giglia, P. Finetti, N. Mahne, L. Pasquali, M. Pedio, G. Selvaggi, G. Naletto, M. G. Pelizzo, and G. Tondello, in *Synchrotron Radiation Instrumentation: Eighth International Conference on Synchrotron Radiation Instrumentation*, edited by T. Warwich *et al.*, AIP Conf. Proc. No. 705 (AIP, Melville, NY, 2004), p. 450.
[20] R. F. C. Farrow, P. W. Sullivan, G. M. Williams, G. R. Jones, and D. C. Cameron, J. Vac. Sci. Technol. **19**, 415 (1981).
[21] A. Ishizaka and Y. Shiraki, J. Electrochem. Soc. **133**, 666 (1986).
[22] For a review, see, for example, G. V. Hansson and R. I. G. Uhrberg, Surf. Sci. Rep. **9**, 197 (1988).
[23] S. Tanuma, C. J. Powell, and D. R. Penn, Surf. Interface Anal. **21**, 165 (1993).
[24] E. Landemark, C. J. Karlsson, Y.-C. Chao, and R. I. G. Uhrberg, Phys. Rev. Lett. **69**, 1588 (1992).
[25] A. Herrera-Gómez, F. S. Aguirre-Tostado, Y. Sun, P. Pianetta, Z. Yu, D. Marshall, R. Droopad, and W. E. Spicer, J. Appl. Phys. **90**, 6070 (2001).
[26] R. Cimino, A. Giarante, K. Horn, and M. Pedio, Europhys. Lett. **32**, 601 (1995); V. De Renzi, R. Biagi, U. del Pennino, M. Pedio, A. Goldoni, and R. Larciprete, Phys. Rev. B **62**, R10657 (2000).
[27] Care was taken in the fit to limit the intensity of each negative doublet component to values below those obtained for the corresponding doublets in the clean surface fit, opportunely multiplied by the normalizing factor obtained from rescaling the clean surface curve intensity to the adsorbate curve intensity.
[28] T.-W. Pi, L.-C. Tien, J.-F. Wen, C.-P. Ouyang, C.-P. Cheng, and J. Hwang, Solid State Commun. **125**, 459 (2003).
[29] F. J. Himpsel, U. O. Karlsson, A. B. McLean, L. J. Terminello, F. M. F. de Groot, M. Abbate, J. C. Fuggle, J. A. Yarmoff, B. T. Thole, and G. A. Sawatzky, Phys. Rev. B **43**, 6899 (1991).
[30] U. O. Karlsson, F. J. Himpsel, J. F. Morar, F. R. McFeely, D. Rieger, and J. A. Yarmoff, Phys. Rev. Lett. **57**, 1247 (1986).

[31] V. M. Bermudez, Appl. Surf. Sci. **161**, 277 (2000).
[32] T. A. Jung, R. R. Schlittler, J. K. Gimzewski, H. Tang, and C. Joachim, Science **271**, 181 (1996); T. A. Jung, R. R. Schlittler, and J. K. Gimzewski, Nature (London) **386**, 696 (1997).
[33] R. A. McKee, F. J. Walker, and M. F. Chisholm, Phys. Rev. Lett. **81**, 3014 (1998).
[34] J. J. Boland and J. H. Weaver, Phys. Today **51**(8), 34 (1998).
[35] J. Wang, J. A. Hallmark, D. S. Marshall, W. J. Ooms, P. Ordejón, J. Junquera, D. Sánchez-Portal, E. Artacho, and J. M. Soler, Phys. Rev. B **60**, 4968 (1999).
[36] See, for example, P. Imperatori, K. Evans-Lutterodt, A. Ippoliti, M. Capozi, M. Pedio, and R. Felici, Appl. Surf. Sci. **123/124**, 636 (1998) and references therein.
[37] A. Franciosi, J. H. Weaver, and D. T. Peterson, Phys. Rev. B **31**, 3606 (1985).
[38] J. D. Denlinger, E. Rotenberg, U. Hessinger, M. Leskovar, and M. A. Olmstead, Phys. Rev. B **51**, 5352 (1995).
[39] W. C. Fan, N. J. Wu, and A. Ignatiev, Phys. Rev. B **42**, 1254 (1990).
[40] R. Z. Bakhtizin, J. Kishimoto, T. Hashizume, and T. Sakurai, J. Vac. Sci. Technol. B **14**, 1000 (1996).
[41] X. Hu, C. A. Peterson, D. Sarid, Z. Yu, J. Wang, D. S. Marshall, R. Droopad, J. A. Hallmark, and W. J. Ooms, Surf. Sci. **426**, 69 (1999).
[42] X. Hu, X. Yao, C. A. Peterson, D. Sarid, Z. Yu, J. Wang, D. S. Marshall, R. Droopad, J. A. Hallmark, and W. J. Ooms, Surf. Sci. **445**, 256 (2000).
[43] A. Herrera-Gómez, P. Pianetta, D. Marshall, E. Nelson, and W. E. Spicer, Phys. Rev. B **61**, 12988 (2000).
[44] T. Ichinokawa, H. Itho, A. Schmid, D. Winau, and J. Kirschner, J. Vac. Sci. Technol. B **12**, 2070 (1994).
[45] H. L. Meyerheim, N. Jedrecy, M. Sauvage-Simkin, and R. Pinchaux, Phys. Rev. B **58**, 2118 (1998).
[46] J. Wang, J. A. Hallmark, D. S. Marshall, W. J. Ooms, P. Ordejón, J. Junquera, D. Sánchez-Portal, E. Artacho, and J. M. Soler, Phys. Rev. B **60**, 4968 (1999).